Self-assembly of 5,6-dihydroxyindole-2-carboxylic acid: polymorphism of a eumelanin building block on Au(111)†

F. De Marchi, ‡[a] G. Galeotti, ‡[a] M. Simenas, [b] P. Ji,[a,c] L. Chi, [c] E. E. Tornau,[d] A. Pezzella, [e,f] J. MacLeod, *[g] M. Ebrahimi *§[a] and F. Rosei *[a,h]

Investigating two-dimensional (2D) self-assembled structures of biological monomers governed by intermolecular interactions is a prerequisite to understand the self-assembly of more complex biomolecular systems. 5,6-Dihydroxyindole carboxylic acid (DHICA) is one of the building blocks of eumelanin – an irregular heteropolymer and the most common form of melanin which has potential applications in organic electronics and bioelectronics. By means of scanning tunneling microscopy, density functional theory and Monte Carlo calculations, we investigate DHICA molecular configurations and interactions underlying the multiple 2D patterns formed on Au(111). While DHICA self-assembled molecular networks (SAMNs) are dominated by the hydrogen bonding of carboxylic acid dimers, a variety of 2D architectures are formed due to the multiple weak interactions of the catechol group. The hydroxyl group also allows for redox reactions, caused by oxidation *via* O_2 exposure, resulting in molecular rearrangement. The susceptibility of the molecules to oxidation is affected by their SAMNs architectures, giving insights on the reactivity of indoles as well as highlighting non-covalent assembly as an approach to guide selective oxidation reactions.

Introduction

The design of new organic materials is inspired by observation of biological systems, in which self-assembled structures are fundamental to the complex functions of living cells.[1,2] Scanning tunneling microscopy (STM) allows the imaging of these systems on atomically flat surfaces at the nanoscale, in a reduced complexity environment, probing the interfacial and intermolecular interactions that regulate the self-assembly processes. This has enabled progress towards the fundamental understanding of these interactions, leading to valuable insights into the macroscopic behaviour of biological systems.[3,4] In addition, these investigations further improve our ability to predict *a priori* the outcome of self-assembly processes,[5] which is a critical step toward engineering the properties of 2D nanostructures. For example, the investigation of the nucleic acid self-assembly on Au(111) helped unravel the molecular recognition process in RNA strands,[6] while at the same time laid the foundation for the formation of 2D nucleic acid oligomers.[7,8]

In this framework, we investigated the self-assembly of the monomers of eumelanin – an elusive class of black insoluble polymers derived biogenetically from tyrosine, which exist in human and mammalian skin, hair, eyes as well as in cephalopod ink.[9,10] Eumelanin's unique characteristics, such as strong optical absorption and hydration-dependent electrical conductivity,[11] have motivated research towards its potential application in organic electronics and bioelectronics.[12–14] However, in depth study of eumelanin is hampered by its chemical intractability and the multiple cross-linked bonds that its building blocks form upon polymerization.[15,16] Despite extensive experimental studies, the relation between the structure,

[a]*Centre Energie, Materiaux et Telecommunications, Institut National de la Recherche Scientifique, 1650 Boulevard Lionel-Boulet, Varennes, QC, Canada J3X 1S2. E-mail: maryam.ebrahimi@emt.inrs.ca, rosei@emt.inrs.ca*
[b]*Faculty of Physics, Vilnius University, Saulėtekio 9, LT-10222 Vilnius, Lithuania*
[c]*Jiangsu Key Laboratory for Carbon-Based Functional Materials & Devices, Institute of Functional Nano & Soft Materials, Soochow University, Suzhou 215123, PR China*
[d]*Semiconductor Physics Institute, Center for Physical Sciences and Technology, Saulėtekio 3, LT-10222 Vilnius, Lithuania*
[e]*Institute for Polymers, Composites and Biomaterials (IPCB), CNR, Via Campi Flegrei 34, I-80078 Pozzuoli, NA, Italy*
[f]*National Interuniversity Consortium of Materials Science and Technology (INSTM), Florence 50121, Italy*
[g]*School of Chemistry, Physics and Mechanical Engineering and Institute for Future Environments, Queensland University of Technology (QUT), 2 George Street, Brisbane, 4001 QLD, Australia. E-mail: jennifer.macleod@qut.edu.au*
[h]*Institute for Fundamental and Frontier Science, University of Electronic Science and Technology of China, Chengdu 610054, PR China*
†Electronic supplementary information (ESI) available. See DOI: 10.1039/c8nr09810g
‡These authors contributed equally.
§Current address: Physics Department E20, Technical University of Munich, James-Franck-Str.1, D-85748 Garching, Germany.

composition, and aggregation of eumelanin is still an intriguing open question.[17]

To shed light upon the interactions between eumelanin monomers, we deposited indole molecules on a surface to investigate the effect of each functional group on the self-assembly process. As we have seen for indole 2-carboxylic acid (I2CA), regardless of the preparation condition, a head–head dimer pair is formed by hydrogen bonding between two carboxylic groups that are arranged in lamellae stabilized by weak side interactions between the indole backbones.[18] For 5,6-dihydroxyindole (DHI), the presence of two hydroxyls in *ortho* position on the phenyl ring (catechol) opens the door to redox reactions.[19] As such, DHI molecules generate metal–organic complexes on silver, while on gold, a covalent dimer of DHI is formed at room temperature (RT).[20–22]

To further extend this investigation, here we report our results regarding the deposition of 5,6-dihydroxyindole-2-carboxylic acid (DHICA) on Au(111) in ultra-high vacuum (UHV) conditions, studying the intermolecular interactions that lead to the formation of DHICA non-covalent 2D nanostructures. DHICA is another intermediate in the biosynthesis of eumelanin which presents the functional groups of both the aforementioned molecules: a carboxylic acid and a catechol similar to I2CA and DHI, respectively (Fig. 1a). Compared to I2CA and DHI, the presence of both functional groups in DHICA increases the possible number of interactions, allowing the creation of self-assembled molecular networks (SAMNs) with different bonding motifs (Fig. 1b and c).

When exposed to O_2,[23] DHI undergoes an oxidation in which catechol group converts into quinone. Here we show that the susceptibility to this process in DHICA is perturbed by the carboxyl group as its presence affects the redox potential of the molecule.[24] In addition, the position of the –COOH on the pyrrole ring of DHICA avoids the formation of a planar covalent dimer, which was previously witnessed for DHI on Au(111). We show that DHICA SAMNs can be affected by exposure to O_2 on Au, triggering a phase transition toward more complex structures reminiscent of the mixed DHI/indolequinone (IQ) phases.[23,25,26]

We used STM to gain information about the network architecture, and density functional theory (DFT) as well as Monte Carlo (MC) calculations to corroborate our interpretation of the molecular structures.

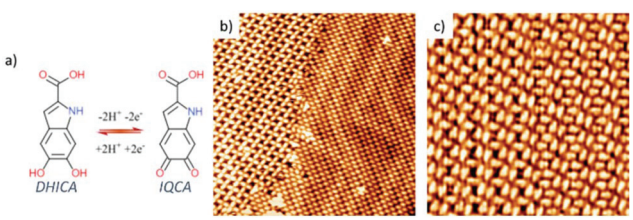

Fig. 1 (a) DHICA oxidation into indolequinone carboxylic acid (IQCA). STM images of the DHICA self-assembled networks on Au(111): (b) 30 × 30 nm^2 open lattice and brick wall phase (I_t = −0.1 nA, V_t = −0.9 V) and (c) 18 × 18 nm^2 ladder and filled ladder phase (I_t = −0.1 nA, V_t = −0.3 V).

Experimental

DHICA was obtained commercially (Toronto Research Chemicals) and also synthesized by reacting L-DOPA with $K_3Fe(CN)_6$ and $NaHCO_3$.[27] The purity of the chemical was 95+%, and no significant change in the data was witnessed between different manufacturers. DHICA powder was stored at −20 °C to avoid polymerization.

All the experiments were performed under UHV conditions in a system with a base pressure of 10^{-10} mbar. The Au(111) surface (Princeton Scientific Corp.) was cleaned by sequential sputtering (0.8 to 1.2 keV at 10^{-5} mbar of Ar for 15 minutes) and annealing (480 °C for 30 minutes) prior to deposition. DHICA was deposited on the surface in a Molecular Beam Epitaxy (MBE) chamber using an effusion (Knudsen) cell. The evaporator was kept at 85 °C for 60 minutes to achieve monolayer coverage on Au(111). The STM imaging was performed using a SPECS Aarhus 150 STM.

To trigger oxidation, samples were exposed to gaseous O_2 by dosing through a leak valve to a pressure of 10^{-5} mbar for 30 minutes.

STM images were analyzed using WSxM software.[28] The images were calibrated using the known Au(111) lattice constant, either from the same image or from images of the clean surface acquired on the same day. Additional details on how the lattice correction was performed are reported in section 1 of the ESI.†

DFT calculations were performed with the Vienna *Ab initio* Simulation Package (VASP).[29,30] The calculations were carried out using the Perdew–Burke–Ernzerhof[31] approximation (PBE) of the exchange–correlation potential, the projector augmented wave (PAW) method,[32,33] and a plane-wave basis set with an energy cut-off of 450 eV. DFT-D3 method of Grimme,[34,35] was applied to account for the dispersion forces, the non-covalent interactions between the molecules. For the simulations of the reported SAMNs, the structures were optimized in the gas phase in which all atoms were relaxed. All the calculations were performed at the gamma point until the net force on each atom was less than 0.02 eV Å^{-1} and the energy change between the two steps was smaller than 0.00001 eV. The optimized structures are presented using VESTA software.[36] Unless stated otherwise, the reported energies are per molecule. The supercell dimensions were taken from the experimental data (Table 1).

The bonding energies of the dimer and trimer DHICA arrangements required for MC simulations were performed

Table 1 Lattice parameters and molecular density for the phases reported in Fig. 2 and 3

	u (nm)	v (nm)	θ (°)	Density (mol nm^{-2})
Open lattice	1.83	1.83	92	1.20
Brick Wall	0.74	2.06	133	1.79
Ladder	1.25	2.05	125	1.43
Mixed	1.25	3.05	98	1.32
Filled ladder	1.23	2.27	110	1.52

using B3LYP functional and 6-31G(d,p) basis set with DFT-D3 correction[34,35] included. To mimic the planar arrangement, the out-of-plane relaxation of the carbon atoms was restrained.

MC simulations[37] were performed using the Metropolis algorithm and Kawasaki dynamics keeping the molecular concentration fixed close to the concentration value of the ideal phases. A square lattice with the periodic boundary conditions of size $L \times L$ (L = 50–100) was implemented. A randomly selected molecule was allowed to rotate and jump into an unoccupied lattice site with a probability $P = \min[1, e^{(-\Delta E/kT)}]$, where ΔE is the energy difference between the final (after the jump) and the initial (before the jump) state of the system. The Boltzmann constant and temperature are denoted by k and T, respectively. Up to 10^7 MC steps per site were performed to ensure proper equilibration at each temperature.

Results and discussion

Once deposited on Au(111), DHICA molecules self-assemble into a number of different motifs, with multiple phases, often simultaneously present on the surface. The most abundant ones are shown in Fig. 2. In all the phases, the unaltered herringbone reconstruction of Au(111) can be seen in the STM images, indicating that the interactions between the molecule and substrate are not strong enough to perturb the surface reconstruction.[38]

The most commonly imaged assembly is presented in Fig. 2a, which we refer to as the open lattice phase. DHICA forms dimer couples, disposed in a square lattice (u = 1.83 ± 0.05 nm, v = 1.83 ± 0.05 nm, θ = 92 ± 3°), forming large 2D domains. Each dimer is oriented almost perpendicular to its neighbours, with its extremities pointing towards the middle of the neighbouring pairs. These observations suggest that the phase is stabilized by the hydrogen bonding between carboxylic groups, as well as being further strengthened by the intermolecular interactions between the catechol and the carboxyl, as shown in Fig. 2a and d.

DHICA molecules also self-assemble in a brick wall structure, presented in Fig. 2b, with lattice parameters u = 0.74 ± 0.05 nm, v = 2.06 ± 0.05 nm, θ = 133 ± 3°. In this phase, DHICA molecules are arranged in a tightly packed linear conformation. From the STM images it is not clear how each single molecule is disposed, since both head–head and head–tail conformations could match the unit cell. By comparing the cohesive energy of the two systems simulated by DFT (Fig. 2e and Fig. S2†), we find that the head–head conformation is more stable by 6.0 kcal mol^{-1}.

The last major structure, which we refer to as the ladder phase, incorporates DHICA molecules in a conformation similar to the open lattice, composed of perpendicular rows of monomers and dimers disposed to form small porous square in a chain-like motif (u = 1.25 ± 0.05 nm, v = 2.05 ± 0.05 nm, θ = 125± 3°, Fig. 2c). DFT simulations show that this structure presents bonding motifs common to both the other two self-assembled phases: the molecules are arranged in carboxylic dimer pairs, stacked side by side similarly to the brick wall, surrounded by molecules with their functional groups pointing toward the –COOH dimer as in the open lattice phase (Fig. 2f).

Furthermore, we observed other phases (Fig. 3 and Fig. S4†) which present bonding motifs very similar to the three phases described in Fig. 2. Such polymorphism is not uncommon for self-assembled molecular system, and different bonding architectures can be obtained by controlling deprotonation with surface temperature,[39] by varying the molecular density on the surface,[40,41] or by adsorption/desorption of additional chemical species.[42,43]

In contrast, in our experiments the annealing of the self-assembled phases does not alter the molecular rearrangement. Multiple phases are often simultaneously present on the same terrace, and even the most close-packed arrangements are obtained for submonolayer coverages (Fig. S5†). Furthermore, a phase transition from a porous to a dense phase does not occur by depositing more molecule *via* subsequent depo-

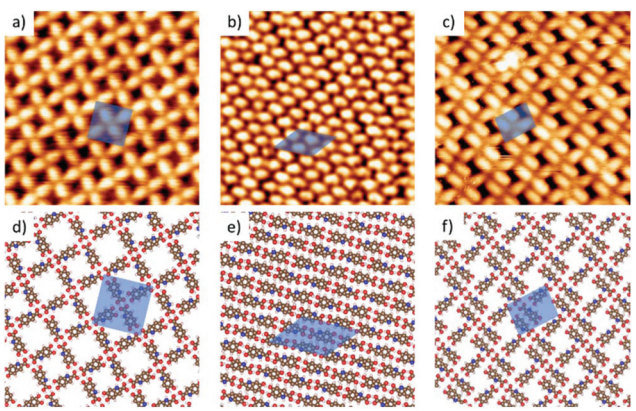

Fig. 2 10 × 10 nm^2 STM images of DHICA on Au (111). (a) Open lattice (I_t = 0.1 nA, V_t =0.9 V), (b) brick wall (I_t = 0.1 nA, V_t = 0.9 V) and (c) ladder phases (I_t = 0.1 nA, V_t = 0.6 V). DFT simulated structures corresponding to a, b, c are shown in d, e, f, respectively.

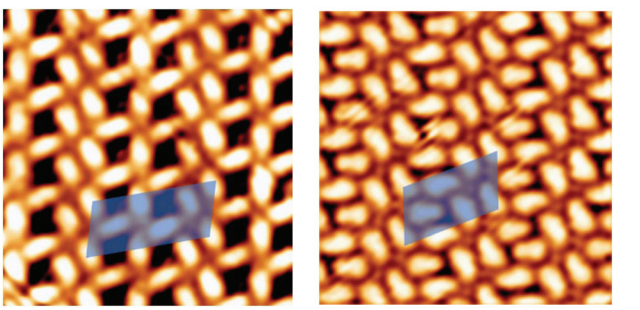

Fig. 3 7 × 7 nm^2 STM images of two less common self-assembled structures of DHICA on the Au(111) surface, that we call (a) mixed (I_t = 0.1 nA, V_t = 1.2 V) and (b) filled ladder (I_t = 0.1 nA, V_t = 0.5 V).

sitions. A possible reason behind the DHICA polymorphism is that we are instead looking into a multicomponent system, with the molecules partially oxidized on the surface. In fact, it has been shown that by changing the ratio between the components of the molecular overlayer, different self-assembled phases can be obtained.[44,45]

On the other hand, coexistence of multiple phases is not limited to multi-components systems. The molecular interactions that drive the self-assembly process toward different outcomes could be balanced by one another; as a consequence, there would be no predominance of a given phase with respect to another.[46] The presence of multiple functional groups may support this hypothesis and explain the observed molecular polymorphism. Taking a closer look at the bonding geometries of the observed phases, it is apparent that in all cases DHICA is stabilized through strong interactions between the carboxyl groups. The reason can be elucidated by comparing the energies of different hydrogen bonds (Fig. 4), where the cyclic –COOH dimer is at least twice as strong as the other interactions. On the other hand, the catechol group can adopt

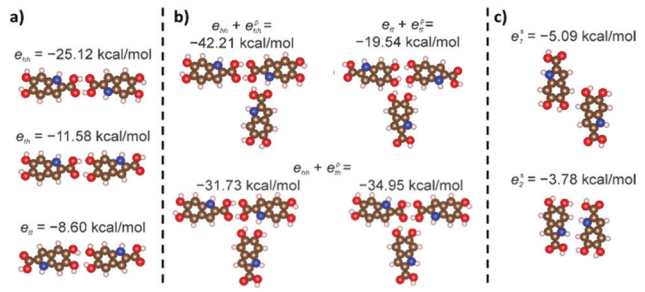

Fig. 4 DFT calculation of the bonding energies per molecule between DHICA molecules in (a) axial, (b) perpendicular and (c) side arrangements. In the denotations of dimeric interaction energies, subscripts "hh", "th" and "tt" are attributed to carboxyl–carboxyl, carboxyl–catechol and catechol–catechol interactions. Superscripts "p" and "s" denote perpendicular and side arrangements of the molecules.

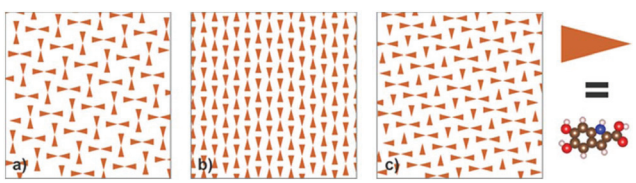

Fig. 5 The ordered structures of DHICA obtained by MC calculations: (a) open lattice, (b) brick wall, and (c) ladder phases.

several different bonding conformations to form hydrogen bonds, either linear with another catechol or perpendicular by interaction with the nitrogen and oxygen of a neighbouring DHICA. These catechol bonding arrangements are rather close in energy, so multiple phases would be accessible at RT, which is consistent with our experimental observations.

To further support this claim, we performed MC simulations of DHICA self-assembly using a four-state statistical model which includes axial, perpendicular and side dimeric interactions between the molecules (see ESI section 3†). Similar models were previously applied to study the ordering of other molecules, including DHI.[23,47–49]

We were able to obtain the open lattice, brick wall and ladder experimental phases (Fig. 5) by MC simulation, using slightly different interaction energies as compared with the gas phase DFT calculated energies (Fig. 4). However, we tried to keep the energy parameters (reported in Table 2) as close as possible to the DFT results. It should be noted that the set of parameters for the brick wall phase almost coincides with the values determined by DFT except for smaller e^{p}_{hh} (DFT value is −17.09 kcal mol^{-1}). The very close sets of energies support the idea that the polymorphism of DHICA at RT is due to similar interaction energies of these phases rather than different redox state of the molecule. While this is in agreement with our previous study of DHI,[23] where we did not observe any catechol-to-quinone oxidation conversion for the adsorbed molecules on the gold surface, we cannot exclude the presence of different redox forms of DHICA based only on the simulation results.

To evaluate if the network polymorphism is related to different oxidation states ratios in the molecular assembly, we attempted to trigger the oxidation of the catecholic part of the molecule by exposing the molecule to O_2 gas, up to the highest pressure that can sustain UHV conditions. As reported in the literature,[50] the partial pressure of oxygen adopted for such experiments (up to 10^{-5} mbar for 30 minutes) is not high enough to have a significant effect on the clean surface at RT.

We found that the exposure of DHICA/Au(111) samples to O_2 leads to several outcomes, depending on the starting phase. Similar to our previous observation on the DHI covalent dimer phase,[23] the DHICA open lattice phase is found to be unaffected by O_2 exposure (Fig. S6a†). The other phases are more strongly affected, becoming disordered as they are exposed to increasing partial pressures of O_2. A phase transition occurs after exposing the molecule to 10^{-5} mbar of O_2, producing a structure with dimer pairs arranged in rows, separated by thin lines that could correspond to the diffusing species (Fig. S7b†).[51]

Table 2 Energy parameters for three DHICA/Au(111) self-assembled networks. Values are reported in kcal mol^{-1}

	e_{hh}	e_{ht}	e_{tt}	e^{p}_{hh}	e^{p}_{th}	e^{p}_{tt}	e^{s}_{1}	e^{s}_{2}
Open lattice	−25.1	−8.8	−6.3	−11.3	−13.8	−5.0	−3.8	−3.8
Brick Wall	−25.1	−11.6	−8.5	−12.6	−10.0	−5.0	−5.0	−5.0
Ladder	−25.1	−8.8	−6.3	−12.6	−10.0	−5.0	−5.0	−3.8

In contrast to the SAMNs unexposed to oxygen, annealing the disordered phases obtained after O_2 exposure leads to a rearrangement of the SAMNs. After thermal annealing at 100 °C, oxygen-exposed DHICA rearranges into a complex honeycomb structure lattice (u = 3.85 ± 0.1 nm, v = 3.85 ± 0.1 nm, θ = 120 ± 3°) whose unit cell contains 18 molecules, as shown in Fig. 6. Molecules are arranged in a flower-like circular structure, forming two concentric rings: six molecules are located at the centre of the structure, pointing inward toward the centre of the honeycomb, while twelve more are closely packed to form a second concentric ring. The molecules in the outer ring are oriented to accommodate the formation of linear dimer pairs, in an arrangement reminiscent of the ladder structure obtained at RT. In contrast to a similar cyclic structure formed from I2CA,[52] we notice that we have high symmetry (without any apparent chirality) in the assembly. This suggests that the central molecular flower-like arrangement may not arise from hydrogen bonding of the carboxylic moieties, since that has been observed to break the symmetry and induce a chiral twist. Another possible interpretation for this configuration is that the molecules are deprotonated, and six of them are coordinated around one or more Au adatoms, in a conformation similar to the one observed for 1,3,5-benzenetricarboxylic acid on Ag(111) by Lipton-Duffin *et al.*[53] This hypothesis is further strengthened by lower bias STM images that show the presence of a dot-like feature at the centre of the flower-like structure, that can be inferred to be related to a gold adatom. Although the carboxylic group may deprotonate after annealing,[54,55] on gold surfaces this phenomenon has not been reported,[56,57] probably because the used precursors desorb before the required temperature could be achieved.

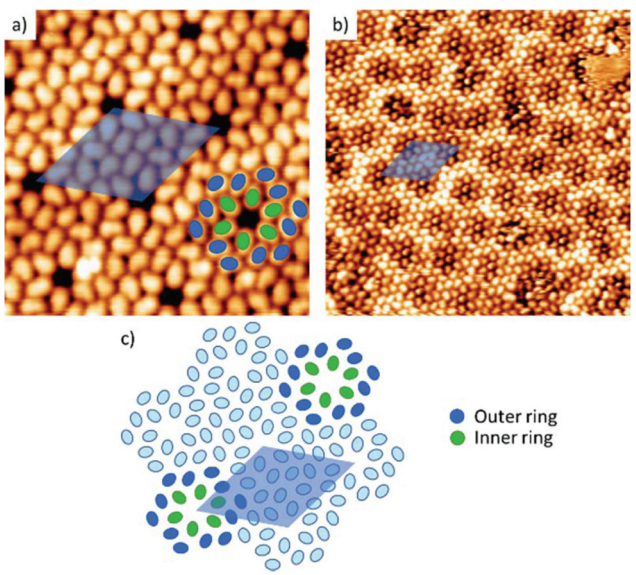

Fig. 6 STM image of DHICA/Au(111) after exposure to O_2, followed by annealing. (a) 9 × 9 nm^2 image (I_t = 1.1 nA, V_t = 1.7 V). (b) 20 × 20 nm^2 (I_t = −1.0 nA, V_t = −1.1 V). (c) Proposed model for the molecular disposition of phase (b).

Furthermore, we witness no change when the annealing step is performed without previous O_2 exposure.

The deprotonation could have instead taken place on the hydroxyl moieties. In fact, the difference in contrast between the molecules composing the central structure and the one in their surroundings (Fig. 6a and b), suggests that these inner cycle molecules may be in a different chemical state than their outer cycle counterparts. In line with what is observed for DHI,[23] in which the catechol and quinone forms of the molecule show a different STM contrast, this suggests that a different redox form of DHICA can be formed after exposure to O_2.

We can therefore hypothesize that DHICA molecules are still in their catechol form when deposited on the Au(111) surface. Following the O_2 exposure part of the molecules have their catechol group oxidized into quinone, which reduces their capability to form hydrogen bonds and leads to an increased disorder in the molecular overlayer. The additional annealing step allows the molecule to diffuse on the surface and triggers the phase transition into the flower structure. This puts DHICA in contrast with its counterpart, DHI, which is stabilized through covalent dimerization on Au(111) at RT and does not convert into quinone. It is interesting to note how the open lattice phase, which present a more porous structure and relies mainly on the carboxylic cyclic hydrogen bond, is resistant to oxidation even when exposed to O_2 with a pressure as high as 10^{-5} mbar.

Conclusions

We studied the self-assembly of DHICA on Au(111), with the goal of investigating how the interaction between the carboxyl and catechol groups drive the self-assembly process. Once on the surface, DHICA molecules rearrange in several polymorphs with different symmetries and packing densities. However, various DHICA SAMNs share a number of similar bonding motifs, suggesting that the self-assembly is driven mainly by the formation of hydrogen bonds between carboxylic acids, which marks the most stable intermolecular interaction of DHICA.

The formation of multiple self-assembled phases can be attributed to the relatively weak molecule–substrate interactions, under which the molecules do not react. The molecules remain in their catechol form, exhibiting multiple non-covalent bonding configurations allowed by their functional groups. While the carboxylic cyclic dimer is a feature of all the formed networks, the catechol group participates in a range of different bonding motifs. Our DFT calculations suggest that these geometries have similar interaction energies. MC simulations of the DHICA systems show how even slight perturbations to the relative strength of these interactions can shift the balance, producing the different phases on the surface in line with our experimental observations.

We have also observed that the susceptibility of the molecule to oxidation is affected by the morphology of the formed self-assembled structure. After being exposed to O_2, the open

lattice phase remains unaltered, while others react to form new phases. It is possible to trigger an additional molecular rearrangement upon thermal annealing. This phase may be composed of a mixed redox forms of DHICA that form a metal–organic structure.

Controlled formation of SAMNs, which are prone or resistant to rearrangements following oxidation and annealing, is a promising feature that could form the foundation for the development of sensors or responsive devices. Additional exploration in this arena could lead to implementation of SAMNs in various applications. Moreover, further investigation of similar systems may help to elucidate the fundamental mechanisms underpinning these behaviours which control the architecture of 2D molecular networks.

Conflicts of interest

There are no conflicts to declare.

Acknowledgements

F. D. M. thanks Eduardo di Mauro and Clara Santato for the support and fruitful discussions. This work was supported by the Natural Sciences and Engineering Research Council of Canada (NSERC) through the Discovery Grants program, as well as the Fonds de Recherche du Québec-Nature et Technologies (FRQNT) through a Team Grant. F. R. is grateful to the Canada Research Chair for funding and partial salary support and also acknowledges NSERC for a Discovery Grant, Sichuan province for a 1000 talent short term award and the Government of China for a short-term Chang Jiang scholar award. J. M. M. acknowledges funding from the Australian Research Council (ARC) through DE170101170. DFT computations were performed on the shared Hierarchical Academic Research Computing Network (SHARCNET: http://www.sharcnet.ca) and the Cedar, Graham, and Niagara clusters of Compute/Calcul Canada.

Notes and references

1 G. M. Whitesides, J. P. Mathias and C. T. Seto, *Science*, 1991, **254**, 1312.
2 G. M. Whitesides and M. Boncheva, *Proc. Natl. Acad. Sci. U. S. A.*, 2002, **99**, 4769–4774.
3 A. Schiffrin, A. Riemann, W. Auwärter, Y. Pennec, A. Weber-Bargioni, D. Cvetko, A. Cossaro, A. Morgante and J. V. Barth, *Proc. Natl. Acad. Sci. U. S. A.*, 2007, **104**, 5279–5284.
4 J. Reichert, A. Schiffrin, W. Auwärter, A. Weber-Bargioni, M. Marschall, M. Dell'Angela, D. Cvetko, G. Bavdek, A. Cossaro, A. Morgante and J. V. Barth, *ACS Nano*, 2010, **4**, 1218–1226.
5 C.-A. Palma, M. Cecchini and P. Samorì, *Chem. Soc. Rev.*, 2012, **41**, 3713–3730.
6 R. Otero, W. Xu, M. Lukas, R. E. A. Kelly, E. Lægsgaard, I. Stensgaard, J. Kjems, L. N. Kantorovich and F. Besenbacher, *Angew. Chem.*, 2008, **120**, 9819–9822.
7 R. Otero, M. Schöck, L. M. Molina, E. Lægsgaard, I. Stensgaard, B. Hammer and F. Besenbacher, *Angew. Chem., Int. Ed.*, 2005, **44**, 2270–2275.
8 S. Xu, M. Dong, E. Rauls, R. Otero, T. R. Linderoth and F. Besenbacher, *Nano Lett.*, 2006, **6**, 1434–1438.
9 M. S. Blois, in *Photochemical and Photobiological Reviews: Volume 3*, ed. K. C. Smith, Springer US, Boston, MA, 1978, pp. 115–134.
10 E. Di Mauro, R. Xu, G. Soliveri and C. Santato, *MRS Commun.*, 2017, **7**, 141–151.
11 A. A. R. Watt, J. P. Bothma and P. Meredith, *Soft Matter*, 2009, **5**, 3754–3760.
12 M. D'Ischia, A. Napolitano, A. Pezzella, P. Meredith and T. Sarna, *Angew. Chem., Int. Ed*, 2009, **48**, 3914–3921.
13 P. Meredith and T. Sarna, *Pigm. Cell Melanoma Res.*, 2006, **19**, 572–594.
14 J. Wünsche, Y. Deng, P. Kumar, E. Di Mauro, E. Josberger, J. Sayago, A. Pezzella, F. Soavi, F. Cicoira, M. Rolandi and C. Santato, *Chem. Mater.*, 2015, **27**, 436–442.
15 M. D'Ischia, A. Napolitano and A. Pezzella, *Eur. J. Org. Chem.*, 2011, **2011**, 5501–5516.
16 S. Hong, Y. S. Na, S. Choi, I. T. Song, W. Y. Kim and H. Lee, *Adv. Funct. Mater.*, 2012, **22**, 4711–4717.
17 M. L. Tran, B. J. Powell and P. Meredith, *Biophys. J.*, 2006, **90**, 743–752.
18 F. De Marchi, D. Cui, J. Lipton-Duffin, C. Santato, J. M. MacLeod and F. Rosei, *J. Chem. Phys.*, 2015, **142**, 101923.
19 J. Yang, M. A. Cohen Stuart and M. Kamperman, *Chem. Soc. Rev.*, 2014, **43**, 8271–8298.
20 S. J. Orlow, M. P. Osber and J. M. Pawelek, *Pigm. Cell Melanoma Res.*, 1992, **5**, 113–121.
21 M. D'Ischia, A. Napolitano, A. Pezzella, E. J. Land, C. A. Ramsden and P. A. Riley, in *Advances in Heterocyclic Chemistry*, ed. R. K. Alan, Academic Press, 2005, vol. 89, pp. 1–63.
22 L. Panzella, A. Pezzella, M. Arzillo, P. Manini, A. Napolitano and M. D'Ischia, *Tetrahedron*, 2009, **65**, 2032–2036.
23 F. De Marchi, G. Galeotti, M. Simenas, E. E. Tornau, A. Pezzella, J. MacLeod, M. Ebrahimi and F. Rosei, *Nanoscale*, 2018, **10**, 16721–16729.
24 R. Xu, C. T. Prontera, E. Di Mauro, A. Pezzella, F. Soavi and C. Santato, *APL Mater.*, 2017, **5**, 126108.
25 L. Giovanelli, O. Ourdjini, M. Abel, R. Pawlak, J. Fujii, L. Porte, J.-M. Themlin and S. Clair, *J. Phys. Chem. C*, 2014, **118**, 14899–14904.
26 S. Clair, M. Abel and L. Porte, *Angew. Chem., Int. Ed.*, 2010, **49**, 8237–8239.
27 A. Corani, A. Huijser, T. Gustavsson, D. Markovitsi, P.-Å. Malmqvist, A. Pezzella, M. D'Ischia and V. Sundström, *J. Am. Chem. Soc.*, 2014, **136**, 11626–11635.
28 I. Horcas, R. Fernandez, J. M. Gomez-Rodriguez, J. Colchero, J. Gomez-Herrero and A. M. Baro, *Rev. Sci. Instrum.*, 2007, **78**, 013705.

29 G. Kresse and J. Hafner, *Phys. Rev. B: Condens. Matter Mater. Phys.*, 1993, **47**, 558–561.
30 G. Kresse and J. Furthmüller, *Phys. Rev. B: Condens. Matter Mater. Phys.*, 1996, **54**, 11169–11186.
31 J. P. Perdew, M. Ernzerhof and K. Burke, *J. Chem. Phys.*, 1996, **105**, 9982–9985.
32 P. E. Blöchl, *Phys. Rev. B: Condens. Matter Mater. Phys.*, 1994, **50**, 17953–17979.
33 G. Kresse and D. Joubert, *Phys. Rev. B: Condens. Matter Mater. Phys.*, 1999, **59**, 1758–1775.
34 S. Grimme, *J. Comput. Chem.*, 2006, **27**, 1787–1799.
35 S. Grimme, J. Antony, S. Ehrlich and H. Krieg, *J. Chem. Phys.*, 2010, **132**, 154104.
36 K. Momma and F. Izumi, *J. Appl. Crystallogr.*, 2011, **44**, 1272–1276.
37 D. Landau and K. Binder, *A Guide to Monte Carlo Simulations in Statistical Physics*, Cambridge University Press, 2005.
38 T. A. Pham, F. Song, M.-T. Nguyen, Z. Li, F. Studener and M. Stöhr, *Chem. – Eur. J.*, 2016, **22**, 5937–5944.
39 Z. Tao, T. Wang, D. Wu, L. Feng, J. Huang, X. Wu and J. Zhu, *Chem. Commun.*, 2018, **54**, 7010–7013.
40 F. Cheng, X.-J. Wu, Z. Hu, X. Lu, Z. Ding, Y. Shao, H. Xu, W. Ji, J. Wu and K. P. Loh, *Nat. Commun.*, 2018, **9**, 4871.
41 N. Thi Ngoc Ha, T. G. Gopakumar and M. Hietschold, *J. Phys. Chem. C*, 2011, **115**, 21743–21749.
42 A. Ciesielski, S. Lena, S. Masiero, G. P. Spada and P. Samorì, *Angew. Chem., Int. Ed.*, 2010, **49**, 1963–1966.
43 M. Wriedt, A. A. Yakovenko, G. J. Halder, A. V. Prosvirin, K. R. Dunbar and H.-C. Zhou, *J. Am. Chem. Soc.*, 2013, **135**, 4040–4050.
44 S. Lei, K. Tahara, J. Adisoejoso, T. Balandina, Y. Tobe and S. De Feyter, *CrystEngComm*, 2010, **12**, 3369–3381.
45 S. Lei, K. Tahara, Y. Tobe and S. De Feyter, *Chem. Commun.*, 2010, **46**, 9125–9127.
46 B. E. Hirsch, K. P. McDonald, A. H. Flood and S. L. Tait, *J. Chem. Phys.*, 2015, **142**, 101914.
47 M. Šimėnas and E. E. Tornau, *J. Chem. Phys.*, 2013, **139**, 154711.
48 M. Šimėnas, A. Ibenskas and E. E. Tornau, *J. Phys. Chem. C*, 2015, **119**, 20524–20534.
49 P. Szabelski, D. Nieckarz and W. Rżysko, *J. Phys. Chem. C*, 2017, **121**, 25104–25117.
50 N. Saliba, D. H. Parker and B. E. Koel, *Surf. Sci.*, 1998, **410**, 270–282.
51 M. Marschall, J. Reichert, K. Seufert, W. Auwärter, F. Klappenberger, A. Weber-Bargioni, S. Klyatskaya, G. Zoppellaro, A. Nefedov, T. Strunskus, C. Wöll, M. Ruben and J. V. Barth, *ChemPhysChem*, 2010, **11**, 1446–1451.
52 N. A. Wasio, R. C. Quardokus, R. D. Brown, R. P. Forrest, C. S. Lent, S. A. Corcelli, J. A. Christie, K. W. Henderson and S. A. Kandel, *J. Phys. Chem. C*, 2015, **119**, 21011–21017.
53 J. Lipton-Duffin, M. Abyazisani and J. MacLeod, *Chem. Commun.*, 2018, **54**, 8316–8319.
54 H.-Y. Gao, P. A. Held, M. Knor, C. Mück-Lichtenfeld, J. Neugebauer, A. Studer and H. Fuchs, *J. Am. Chem. Soc.*, 2014, **136**, 9658–9663.
55 J. V. Barth, J. Weckesser, N. Lin, A. Dmitriev and K. Kern, *Appl. Phys. A*, 2003, **76**, 645–652.
56 T. Yokoyama, T. Kamikado, S. Yokoyama and S. Mashiko, *J. Chem. Phys.*, 2004, **121**, 11993–11997.
57 S. Clair, S. Pons, A. P. Seitsonen, H. Brune, K. Kern and J. V. Barth, *J. Phys. Chem. B*, 2004, **108**, 14585–14590.